Physica B 407 (2012) 2825–2828

Contents lists available at SciVerse ScienceDirect

Physica B

journal homepage: www.elsevier.com/locate/physb

Low temperature electron transport in phosphorus-doped ZnO films grown on Si substrates

K. Zhang [a,b], M.R. Hao [a], W. Guo [b], T. Heeg [c], D.G. Schlom [c], W.Z. Shen [a,*], X.Q. Pan [b]

[a] Laboratory of Condensed Matter Spectroscopy and Opto-Electronic Physics, and Key Laboratory of Artificial Structures and Quantum Control (Ministry of Education), Department of Physics, Shanghai Jiao Tong University, Shanghai 200240, China
[b] Department of Materials Science and Engineering, University of Michigan, Ann Arbor, MI 48109, USA
[c] Department of Materials Science and Engineering, Cornell University, Ithaca, NY 14853, USA

ARTICLE INFO

Article history:
Received 5 April 2012
Accepted 17 April 2012
Available online 24 April 2012

Keywords:
Zinc oxide
Pulsed laser deposition
Dislocation
Electron dephasing

ABSTRACT

Low temperature magneto-transport properties and electron dephasing mechanisms of phosphorus-doped ZnO thin films grown on (1 1 1) Si substrates with Lu_2O_3 buffer layers using pulsed laser deposition were investigated in detail by quantum interference and weak localization theories under magnetic fields up to 10 T. The dephasing length follows the temperature dependence with an index $p \approx 1.6$ at higher temperatures indicating electron–electron interaction, yet becomes saturated at lower temperatures. Consistent with photoluminescence measurements and the multi-band simulation of the electron concentration, such behavior was associated with the dislocation densities obtained from x-ray diffraction and mobility fittings, where charged edge dislocations acting as inelastic Coulomb scattering centers were affirmed responsible for electron dephasing. Owing to the temperature independence of the dislocation density, the phosphorus-doped ZnO film maintained a Hall mobility of 4.5 $cm^2 V^{-1} s^{-1}$ at 4 K.

1. Introduction

Zinc oxide (ZnO) is a wide band gap II–VI material with an exciton binding energy of 60 meV, higher than many other compound semiconductors, which leads to possible light emitting applications well above room temperature (RT). The band gap of ZnO can be tuned by dilute alloying with other oxides such as CdO [1], MgO [2] and BeO [3], suggesting its potential in customized short-wavelength optoelectronic devices. The major obstacle to the development of ZnO has been the lack of stable, conductive *p*-type epitaxial layers [4] due to its asymmetric doping limits strongly against *p*-doping [5]. The theoretically promising dopant N has low solubility in ZnO and is often compensated by donors including hydrogen [6] and Zn interstitials [7]. Larger-size elements in group V were studied as alternatives to N, among which P doped ZnO (PZO) has attracted intensive interest in recent years for its transition from as-grown *n*-type to *p*-type conduction after proper thermal annealing [8]. However in these reports, an in-depth discussion is lacking on the electron transport and scattering mechanisms. Previous research has shown that the formation of P_{Zn}–$2V_{Zn}$ complexes which behave as shallow acceptors is vital to the onset of *p*-type conductivity in PZO films [9], while the existence of high density threading dislocations enhances the solubility of P in ZnO and also facilitates the injection of Zn vacancies. In order to better control the performance of PZO based electrical devices, a solid understanding of the interaction between electrons and dislocations in these films is necessary.

In this paper, we report the experimental and theoretical investigation into the microstructure, optical and transport properties of the PZO thin films grown on (1 1 1) Si substrates with epitaxial Lu_2O_3 buffer layers. In addition to temperature dependent carrier concentration and mobility fittings, electron localization effect was studied under low temperatures and strong magnetic fields, where the dephasing length was extracted to analyze the scattering mechanism. The employment of Si substrate, as compared with sapphire in most reports, contributes to the effort of integrating ZnO-based materials with Si optoelectronics.

2. Experimental

A 30 nm Lu_2O_3 buffer layer was first grown on (1 1 1) Si substrate at 700 °C by reactive molecular beam epitaxy (MBE). The 500 nm PZO film was deposited on the buffer layer at 500 °C in 20 mTorr O_2 by pulsed laser deposition (PLD) from a ZnO target doped with 1 wt% P_2O_5. The KrF excimer laser energy was set to 100 mJ per pulse with a repetition rate of 5 Hz. Secondary-ion mass spectroscopy (SIMS) determined that phosphorus distributes uniformly through the

* Corresponding author. Tel./fax: +86 21 54747552.
E-mail address: wzshen@sjtu.edu.cn (W.Z. Shen).

0921-4526/$ - see front matter © 2012 Elsevier B.V. All rights reserved.
http://dx.doi.org/10.1016/j.physb.2012.04.036

PZO films with a concentration of 2.8×10^{20} cm^{-3}. Microstructure of the films was studied by x-ray diffraction (XRD) using a triple-axis high-resolution BEDE-D1 diffractometer with Cu Kα radiation and by photoluminescence (PL) using a 325 nm Kimmon He–Cd laser and a Jobin-Yvon spectrometer with a photomultiplier tube. The temperature-dependent magnetoconductivity experiments were performed in Van der Pauw configuration using an Oxford Instruments controllable superconductive electromagnet with a liquid-helium-cooled cryostat. The studied films were strictly square shaped with a correction factor equal to 1, and each recorded data point was averaged over eight measurements by rotating the electrodes and reversing both current and magnetic field to eliminate errors from electrode asymmetricity, Nernst effect and Righi–Leduc effect for reliable and repeatable data acquisition.

3. Results and discussion

Fig. 1(a) is the XRD θ-2θ scan pattern of the PZO/Lu_2O_3/Si film, which clearly shows an out-of-plane orientation relationship of $(0\,0\,0\,1)_{PZO}\|(1\,1\,1)_{Lu_2O_3}\|(1\,1\,1)_{Si}$ with no other PZO or impurity peaks observed. Full width at half maximum (FWHM) of the 0002 PZO ω-rocking curve is 1.246°. Agreeing with previous reports on PZO [9,10], the P dopants existing as P_{Zn} antisites are responsible for the XRD peak broadening as they disturb the original ZnO lattice, and for the n-type conduction in as-grown samples discussed below [11]. Dislocations form through the film because of both the lattice mismatch between PZO and Lu_2O_3, and the low mobility of phosphorus atoms in ZnO. The epilayer tilt angle α_Ω and twist angle α_Φ were obtained from the ω-rocking peak broadening of symmetric reflections $000l$ (l=2, 4, 6) [12] and skew symmetric off-axis reflections $10\bar{1}l$ 10 (l=1–5) [13], respectively, as shown in Fig. 1(b) and (c). The dislocation densities with a screw- and edge-component were then calculated from these two mosaic angles to be $N_c=3.9\times10^9$ cm^{-2} and $N_a=2.3\times10^{10}$ cm^{-2}, respectively [14]. It should be noted that a mixed type dislocation may have been counted in both N_c and N_a. The inclination angles and ω–FWHM values of each reflection are summarized in Table 1.

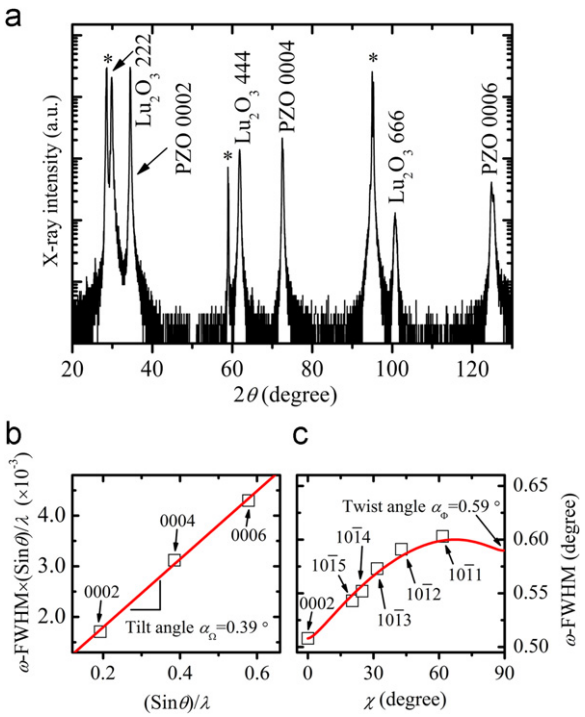

Fig. 1. (a) θ-2θ XRD pattern of a 500 nm PZO film grown on (1 1 1) Si substrate with 30 nm Lu_2O_3 buffer layer. "*" denotes peaks from the Si substrate. (b) The slope of a linear fit of ω–FWHM × Sin θ_B/λ versus Sin θ_B/λ gives the tilt angle α_Ω, where θ_B and λ are the Bragg angle of each peak and the x-ray wavelength, respectively. (c) Fitting the ω–FWHM values of PZO 0002 and five off-axis reflections versus the inclination angle χ gives the twist angle α_Φ at the extrapolation of χ=90°.

The PL spectrum of the PZO film at 12 K is shown in Fig. 2, where the experimental data within the near-band-edge (NBE) range can be well fitted by six Gaussian peaks. Based on temperature-dependent measurements, the peaks at 3.370 and 3.341 eV were assigned to ground-state free exciton (FX) and donor bound exciton (DX) transitions, respectively [15]. ZnO has a longitudinal optical (LO) phonon frequency of 591 cm^{-1} [16], corresponding to an energy separation of ~72 meV, so the three peaks at lower energies were assigned to LO phonon replicas of the DX and FX lines, as indicated in Fig. 2. The two-electron satellite (TES) transition of DX is located at 3.318 eV, and hence the donor binding energy was calculated to be 31 meV in the hydrogenic effective-mass-approach [17]. Emissions from the excited states of free exciton were not observed in this sample because they require highly ordered crystal packing, which is now perturbed by P dopant and consequently dense dislocations.

The as-grown PZO film shows n-type behavior in temperature dependent Hall measurements under B=0–10 T, and its electrical properties at RT are $\rho=0.138\,\Omega$ cm, $n=2.98\times10^{18}$ cm^{-3}, $\mu=15.2$ cm^2 V^{-1} s^{-1}. No obvious dependence on changing B was found in carrier concentration or mobility. The discrepancy between the doping density from SIMS and conducting electron concentration arises from the limited ionization of dopants due to the existing n-type background of ZnO caused by native donors and intrinsic defects and subsequent trapping of free carriers [8,11]. The Lu_2O_3 buffer layer is highly resistive, so there is no concern of possible leakage into the Si substrate. The electron concentration in Fig. 3(a) was fitted by a two-donor/single-acceptor model based on the charge balance equation (CBE) [18]

$$n(T)+N_A=\sum_{i=1}^{2}N_{Di}/[1+n(T)/\phi_i], \quad (1)$$

Table 1
Inclination angles χ and ω–FWHM values of each symmetric and off-axis reflections from XRD ω-rocking curves.

Plane	0002	0004	0006	$10\bar{1}5$	$10\bar{1}4$	$10\bar{1}3$	$10\bar{1}2$	$10\bar{1}1$
χ (°)	0	0	0	20.30	24.81	31.65	42.76	61.60
ω–FWHM (°)	0.508	0.464	0.426	0.543	0.552	0.573	0.591	0.603

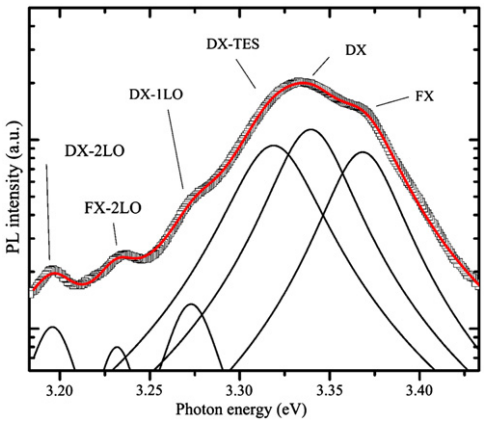

Fig. 2. PL spectrum of the same PZO film at 12 K, which can be well fitted by six Gaussian peaks. The open squares represent experimental data, while the solid curves are calculated results for each peak and their sum.

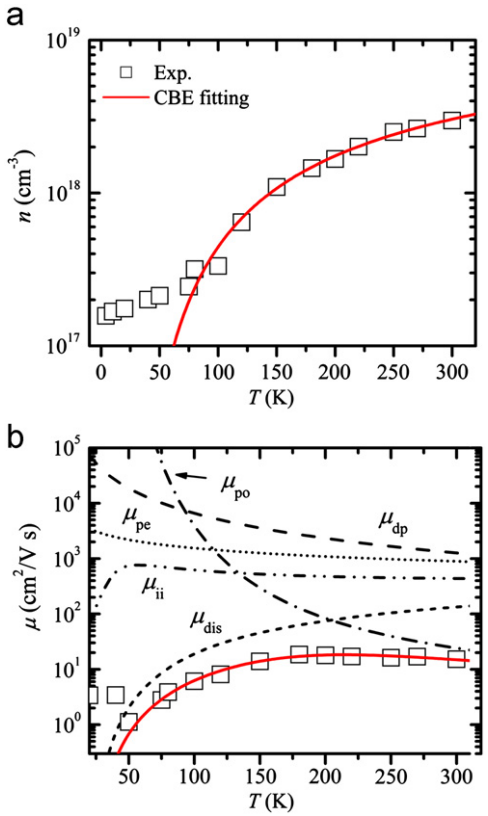

Fig. 3. Temperature dependence of (a) electron concentration and (b) Hall mobility of the same PZO film as in Fig. 1. The open squares represent experimental data recorded at $B=5.5$ T, while the curves are theoretically calculated results.

assuming the first donor is the ionized dopant and the second the common native impurity H in ZnO, where the activation energies of the two donors (which essentially compose ϕ_i) were first estimated by the PL results above and from the literature [17], respectively. A refining fitting yielded a background acceptor concentration $N_A=2.3\times10^{16}\,\mathrm{cm}^{-3}$, and two donor concentrations $N_{D1}=1.6\times10^{19}\,\mathrm{cm}^{-3}$, $N_{D2}=5.6\times10^{17}\,\mathrm{cm}^{-3}$, with donor activation energies of $E_{D1}=29$ meV and $E_{D2}=47$ meV, respectively, consistent with other P-doped ZnO films in the literature [9]. Electrons freeze out at temperatures lower than 50 K, where the experimental data fall off the fitting curve. Bringing the fitted curve of $n(T)$ in Fig. 3(a) to iterative calculation, the Hall mobility can be further resolved by Matthiessen's rule including five scattering mechanisms: ionized impurity (μ_{ii}), deformation potential (μ_{dp}), piezoelectric potential (μ_{pe}), polar optical phonon (μ_{po}), and dislocation (μ_{dis}) scatterings [18,19], as revealed in Fig. 3(b). The explicit expressions and list of constants used in the fitting can be found in Ref. [20]. Apparently, dislocation scattering dominates the mobility behavior within most of the measured temperature range, while polar optical phonon scattering takes over at higher temperatures. The dislocation density extracted from the fitting was $N_{dis}=2.2\times10^{10}\,\mathrm{cm}^{-2}$, agreeing with N_a obtained previously from XRD tests, confirming that the mechanism of mobility reduction is Coulomb scattering at charged edge dislocation lines [19].

A deeper insight into the transport characteristics of the PZO film was realized by studying the electron dephasing behavior, where an unusual electrical transport phenomenon of dephasing length saturation and related scattering mechanism were directly connected with Hall properties and the sample's microstructure discussed above. Fig. 4(a) shows the B dependent conductivity

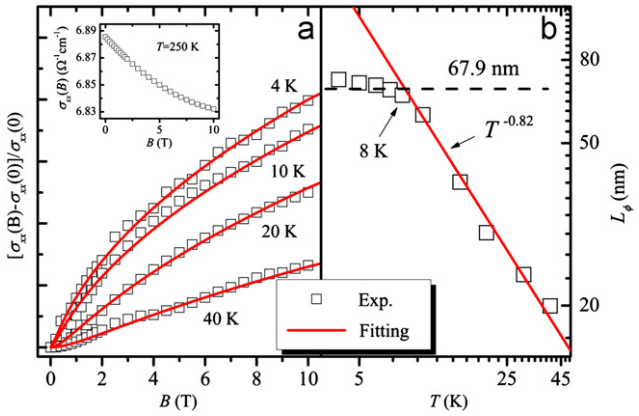

Fig. 4. (a) Magnetic field dependence of conductivity in the PZO film at different temperatures, which shows classical Boltzmann behavior at 250 K (inset), but quantum interference phenomenon at low temperature. The solid curves are fitting results by the DFS model. (b) Temperature dependence of dephasing lengths extracted from the DFS fitting process. The solid curve represents an exponential fit, while the dash line is set at a value corresponding to the edge dislocation density obtained in mobility fitting.

from 0–10 T at different temperatures. The xx component of the conductivity tensor calculated from Hall data normally decreases with increasing B around RT since the magnetic field bends the pathway of conducting electrons when an external bias is applied, as shown in the inset of Fig. 4(a) for $T=250$ K where the magnetoconductivity obeys the classical Boltzmann B^2 law. However, when the temperature decreases to a certain level that the phonons as inelastic scattering sources are largely suppressed, the strong quantum interference of electron waves will cause weak localization effect and reduces the conductivity [21]. In such cases, the magnetic field imposes an additional phase term $\exp[\pm ie\Phi/\hbar]$, Φ being the magnetic flux enclosed by the electron path, to the electron wave and breaks the time-reversal symmetry, which weakens the localization effect and results in the increase of the conductivity. In our sample, the positive magnetoconductivity was observed below 40 K, as revealed in Fig. 4(a) by the normalized change of $\sigma_{xx}(B)$, where it is clearly seen that the quantum interference becomes stronger at lower temperature. The solid curves in good agreement with the experimental data are theoretical calculations by the diffusive Fermi-surface (DFS) theory [22,23],

$$\Delta\sigma(B)=\frac{e^2}{2\pi^2\hbar d}F(\delta,\delta'),$$

$$F(\delta,\delta')=2\sum_{n=0}^{\infty}\left[\ln\left(\frac{\sqrt{n+\delta+1}+\sqrt{n+\delta'+1}}{\sqrt{n+\delta}+\sqrt{n+\delta'}}\right)-\frac{1}{\sqrt{2n+2\delta+1}\sqrt{2n+2\delta'+1}}\right], \quad (2)$$

where d is a characteristic length parameter, $\delta=\hbar/(4eBL_\phi^2)$ and $\delta=\delta+\delta_0$ represent microscopic interactions in the system with δ_0 associated with the coupling energy along z direction. The electron dephasing lengths L_ϕ were extracted during the fitting process at various temperatures and are plotted as open squares in Fig. 4(b).

Dephasing length L_ϕ is the distance that the electron wave can travel before losing its phase memory, which typically occurs at an inelastic scattering event such as electron–phonon interaction or by a cumulative effect of a series of scattering events [24]. The dephasing length usually follows a temperature dependence of $L_\varphi\propto T^{-p/2}$, and the temperature exponent p determines the type

of interaction [25]. An exponential fit of the experimental data above 8 K in Fig. 4(b) gives a temperature exponent of -0.82, or $p \approx 1.6$, which is a sign of Coulomb electron–electron processes [25]. At temperatures below 8 K, however, the dephasing length does not increase with decreasing temperature as fast as predicted, but seems to have been bounded by a certain mechanism. Since electrons are mostly driven to move in directions parallel to the film surface under the Van der Pauw configuration, such mechanism should relate to a scattering source that mainly extends in the vertical orientation. A logical deduction would be the vertically located edge dislocations [19]. The mean distance between two dislocation lines can be computed by the dislocation density N_{dis} obtained in mobility fitting as $1/\sqrt{N_{dis}} = 67.9$ nm, which is drawn as a dash line in Fig. 4(b). The fact that this estimation matches the saturation behavior of the dephasing length considerably well indicates that the edge dislocations may be responsible for breaking the phase coherence of the electron wave. Although dislocation scattering in crystalline semiconductors is often treated as elastic interactions, in doped structures such as our PZO thin film, the dopant atoms are often embedded in the threading dislocations [19], creating potential anomalies in the crystal electric field. Therefore the dislocations could trap free carriers and become charged. Combining with the lattice vibration, these dislocations may act as inelastic Coulomb scattering centers.

Such reasoning suggests that certain electrical properties of the PZO thin film can be controlled by adjusting the growth conditions and hence the defect structure [26]. To obtain larger dislocation spacing, a 1 wt% doped PZO film was grown on (0 0 0 1) sapphire substrate at 800 °C. This film had better structural quality with a lower edge dislocation density $N_a = 4.2 \times 10^9\ cm^{-2}$ which corresponds to a mean spacing of 154.3 nm, while the above $T^{-0.82}$ fitting predicts a dephasing length of 122.7 nm at 4 K. An actual dephasing length of 131.4 nm was experimentally measured from the localization effect, demonstrating that the electron wave was not bounded by the dislocations in this case. On the other hand, no low temperature quantum interference phenomenon was observed in the annealed *p*-type PZO films reported elsewhere [8] because the edge dislocation densities are quite high in these samples ($> 10^{11}\ cm^{-2}$), causing dephasing over a very short distance and hence steady conductivity without evident magnetic field dependence.

The above findings point out both the challenge and opportunity in devices based on phosphorus-doped ZnO thin films. For *p*-type conductance, the P_{Zn}–$2V_{Zn}$ complexes which ionize holes are a direct result from the P dopants and zinc vacancy injection, but the threading dislocations which help accommodate the P atoms that are much larger than O atoms constitute inelastic scattering centers when charged, significantly reducing the carrier mobility ($\sim 1\ cm^2\ V^{-1}\ s^{-1}$ in the reports [8,27]). Therefore a tradeoff must be designed between the doping level and the target mobility. Meanwhile, the mobility of the PZO films does not change drastically with temperature since the dislocations as major scattering centers are temperature independent. For instance, the *n*-type PZO film in Fig. 3 maintained a mobility of $4.5\ cm^2\ V^{-1}\ s^{-1}$ even at 4 K. The *p*-type PZO film obtained by post-deposition annealing that reduces native donor (e.g. oxygen vacancies) concentration has much lower mobility for the lack of holes under low temperature, but is free from localization effects due to short dephasing lengths, thus favorable to higher conductivity. These advantages, together with the radiation hardness of ZnO [28], make PZO a potential candidate for low temperature applications such as in space environments.

4. Conclusion

Low temperature magneto-transport properties of phosphorus-doped (0 0 0 1) ZnO thin films grown on (1 1 1) Si substrates with Lu_2O_3 buffer layers were studied. Threading dislocations which form upon phosphorus doping were identified as major scattering centers, explaining the relatively high mobility under low temperatures, also pointing out a tradeoff for *p*-type doping. Vertical edge dislocations can be charged by trapping free carriers and act as inelastic Coulomb scattering centers, and are affirmed responsible for electron dephasing due to the agreement between the saturation behavior of electron dephasing lengths and the dislocation densities that can be controlled by growth and processing conditions.

Acknowledgments

This work was supported by the National Science Foundation through grant DMR-0907191 and by the Natural Science Foundation of China under contracts 10734020 and 11174202.

References

[1] T. Makino, Y. Segawa, M. Kawasaki, A. Ohtomo, R. Shiroki, K. Tamura, T. Yasuda, H. Koinuma, Appl. Phys. Lett. 78 (2001) 1237.
[2] A. Ohtomo, M. Kawasaki, T. Koida, K. Masubuchi, H. Koinuma, Y. Sakurai, Y. Yoshida, T. Yasuda, Y. Segawa, Appl. Phys. Lett. 72 (1998) 2466.
[3] Y.R. Ryu, T.S. Lee, J.A. Lubguban, A.B. Corman, H.W. White, J.H. Leem, M.S. Han, Y.S. Park, C.J. Youn, W.J. Kim, Appl. Phys. Lett. 88 (2006) 052103.
[4] D.C. Look, B. Claftin, Phys. Status Solidi B 241 (2004) 624.
[5] S.B. Zhang, S.H. Wei, A. Zunger, J. Appl. Phys. 83 (1998) 3192.
[6] C.G. Van de Walle, Phys. Rev. Lett. 85 (2000) 1012.
[7] D.C. Look, G.C. Farlow, P. Reunchan, S. Limpijumnong, S.B. Zhang, K. Nordlund, Phys. Rev. Lett. 95 (2005) 225502.
[8] A. Allenic, W. Guo, Y.B. Chen, M.B. Katz, G.Y. Zhao, Y. Che, Z.D. Hu, B. Liu, S.B. Zhang, X.Q. Pan, Adv. Mater. 19 (2007) 3333.
[9] A. Allenic, W. Guo, Y.B. Chen, Y. Che, Z.D. Hu, B. Liu, X.Q. Pan, J. Phys. D: Appl. Phys. 41 (2008) 025103.
[10] Y.W. Heo, S.J. Park, K. Ip, S.J. Pearton, D.P. Norton, Appl. Phys. Lett. 83 (2003) 1128.
[11] U. Wahl, E. Rita, J.G. Correia, A.C. Marques, E. Alves, J.C. Soares, I. Collaboration, Phys. Rev. Lett. 95 (2005) 215503.
[12] G.K. Williamson, W.H. Hall, Acta Metall. 1 (1953) 22.
[13] V. Srikant, J.S. Speck, D.R. Clarke, J. Appl. Phys. 82 (1997) 4286.
[14] C.G. Dunn, E.F. Koch, Acta Metall. 5 (1957) 548.
[15] H. Tampo, H. Shibata, P. Fons, A. Yamada, K. Matsubara, K. Iwata, K. Tamura, H. Takasu, S. Niki, J. Cryst. Growth 278 (2005) 268.
[16] C.A. Arguello, D.L. Rousseau, S.P.S. Porto, Phys. Rev. 181 (1969) 1351.
[17] B.K. Meyer, H. Alves, D.M. Hofmann, W. Kriegseis, D. Forster, F. Bertram, J. Christen, A. Hoffmann, M. Straßburg, M. Dworzak, U. Haboeck, A.V. Rodina, Phys. Status Solidi B 241 (2004) 231.
[18] D.C. Look, Electrical Characterization of GaAs Materials and Devices, Wiley, New York, 1989.
[19] N.G. Weimann, L.F. Eastman, D. Doppalapudi, H.M. Ng, T.D. Moustakas, J. Appl. Phys. 83 (1998) 3656.
[20] Y.S. Jung, O.V. Kononenko, W.K. Choi, Solid State Commun. 137 (2006) 474.
[21] G. Bergmann, Phys. Rev. B 28 (1983) 2914.
[22] A. Kawabata, J. Phys. Soc. Jpn. 49 (1980) 628.
[23] A. Cassamchenai, D. Mailly, Phys. Rev. B 52 (1995) 1984.
[24] K. Zhang, W.Z. Shen, Appl. Phys. Lett. 92 (2008) 083101.
[25] P.A. Lee, T.V. Ramakrishnan, Rev. Mod. Phys. 57 (1985) 287.
[26] C.H. Ahn, Y.Y. Kim, S.W. Kang, H.K. Cho, Physica B 401 (2007) 370.
[27] S.C. Su, X.D. Yang, C.D. Hu, Physica B 406 (2011) 1533.
[28] D.C. Look, D.C. Reynolds, J.W. Hemsky, R.L. Jones, J.R. Sizelove, Appl. Phys. Lett. 75 (1999) 811.